




Jayesh CHORDIYA <sup>1</sup>, Padmakar DESHMUKH <sup>1</sup>,  
Ram Vinoy SHARMA <sup>2</sup>

## Numerical study on the effect of strategically placed multiple diathermal obstructions within a porous enclosure

Received 4 April 2024, Revised 27 July 2024, Accepted 12 August 2024, Published online 30 September 2024

**Keywords:** porous, natural convection, obstructions, diathermal, strategic positioning

A novel strategy to reduce the convection heat transfer across a differentially heated, fluid-saturated porous enclosure has been reported in the present investigation. This objective is achieved by sequentially and strategically embedding multiple diathermal obstructions within the enclosure. To describe it in short, the strategy is to identify the location of maximum convection strength and place a single obstruction at that location. This strategy is re-applied to find an updated location of maximum convection strength and placing another single obstruction at that newly updated location. Darcy flow model is used to describe the fluid flow in porous media and solved using Successive Accelerated Replacement scheme using finite difference method. The parameters under study are type of obstructions (horizontal, vertical, right-inclined, left-inclined, straight-crossed and inclined-crossed), number of obstructions ( $0 \leq N \leq 10$ ) and modified Rayleigh number ( $100 \leq Ra \leq 2000$ ). The size of obstruction ( $Z$ ) has been fixed at 0.1. Flow and temperature distribution are plotted using streamlines and isotherms. The strength of convection is quantified using Nusselt number and maximum absolute stream function. It has been found that introducing obstructions within a differentially heated porous enclosure weakens the convection strength developed within it and the maximum reduction can be obtained for inclined-cross obstruction.

---

✉ Jayesh CHORDIYA, email: [jayesh.subhash@gmail.com](mailto:jayesh.subhash@gmail.com)

<sup>1</sup>Pimpri Chinchawad College of Engineering, Pune, Maharashtra, India

<sup>2</sup>Department of Mechanical Engineering, National Institute of Technology, Jamshedpur, Jharkhand, India



© 2024, The Author(s). This is an open-access article distributed under the terms of the Creative Commons Attribution (CC-BY 4.0, <https://creativecommons.org/licenses/by/4.0/>), which permits use, distribution, and reproduction in any medium, provided that the author and source are cited.

## 1. Introduction

Natural convection generated within a porous enclosure is among the prominent issues due to its extended usage in numerous applications [1, 2] and in a multitude fields, e.g., nuclear reactors [3], boiling and condensation phenomena [4, 5], geothermal systems [6, 7], waste disposal [8–10], heat exchangers [6, 11, 12], thermal insulation by fibrous materials and safety solar systems. The majority of researches and studies have reported the effect of free convective in porous structures with obstructions/partitions/obstacles placed randomly or at some standard locations. Only a handful of works have focused on understanding the effect of multiple obstructions distributed throughout the porous medium. A couple of former studies have been dealing with single partitions with varying orientations, heated partitions, permeable partitions, etc. Nevertheless, the effect on natural convection produced by multiple partitions and varying orientations embedded within a porous enclosure at strategic locations hasn't yet been reported. Thus, the current study is both novel and original one.

A detailed numerical investigation was conducted by [13] on entropy generation in a natural convection flow developed inside a differentially heated square enclosure filled with water and separated by a corrugated-shaped porous partition. It was reported that a higher amplitude, lower thickness and higher frequency leads to an increase in average Nusselt number. The buoyancy-driven flow and heat transfer within a baffled U-shaped porous enclosure saturated with a nano-fluid subjected to an inclined magnetic field was numerically examined by [14], [15] conducted a numerical study on free convection within a non-Darcy porous duct under local thermal non-equilibrium to study the effect of embedding a single hot obstacle which was horizontally/vertically attached at the heated surface. Moreover, [16] reported a numerical study on natural convection within a non-Darcian porous enclosure under local thermal non-equilibrium embedded with a vertical triple adiabatic obstructions. A minimum length of obstacle is recommended for porous heat exchangers with adiabatic obstacles. Further to this, [17] simulated a three-dimensional Fe<sub>3</sub>O<sub>4</sub>/MWCNT-water hybrid nanofluid flow inside a 3D cubic cavity having porous medium. On the similar lines, [18] conducted investigation on mixed convection of Casson hybrid nanofluids in a lid-driven inclined triangular porous cavity having elliptical obstructions. A free convection flow in an H-shaped nano-fluid enclosure partially filled with non-Darcy porous medium and embedded with heated partitions has been simulated by [19], [20] performed CFD simulation of free convection heat transfer in an inverted T-shaped enclosure with a hybrid nanofluid and a porous partition of two types. It was reported that the averaged Nusselt number could be decreases by a drop in Darcy number ratio, porosity ratio, the Rayleigh number, and the increase in the thermal conductivity ratio. Furthermore, a conjugate study with thick partitions inside porous enclosures has been carried out extensively by [21, 22]. Some specific contributions in understanding the influence of shapes of partition are made by the following authors: [23] presented a study of

corrugated shape, [24] analyzed wavy shape, [25] studied the effect of square-wave shaped partition.

The objective of the current investigation is to curtail the rate of convection heat transfer across a differentially heated porous enclosures. This is achieved by sequentially and strategically embedding multiple obstructions of varying orientations viz., horizontal, vertical, left-inclined, right-inclined, straight-crossed and inclined-cross inside the porous enclosure. It is sought to understand the most effective orientation, the effect of number of obstructions, the effect of Rayleigh number and orientation on strategic location of obstructions and to filter out the most effective configuration.

## 2. Mathematical modeling

A square porous enclosure saturated with fluid and heated differentially is shown in Fig. 1 with each side of length  $L$ . The upper and lower edges are assumed adiabatic. The left wall is relatively cooler ( $T = T_c$ ) while the right wall is relatively hotter ( $T = T_h$ ) such that  $T_c \ll T_h$ . The porous medium is rigid, homogeneous and carries a Newtonian fluid. The flow is steady and laminar. The obstructions embedded inside the enclosure are given five different orientations viz., horizontal, vertical, left-inclined, right-inclined, straight-crossed and inclined-cross and these are assumed to be impermeable, rigid and diathermal. A multiple of such obstructions are embedded sequentially and strategically.  $N$  signifies the number of obstructions and their size is given by  $z$ .  $x_{pm}$  and  $y_{pm}$  gives the location of the midpoint of obstruction in horizontal and vertical coordinates. The left- and

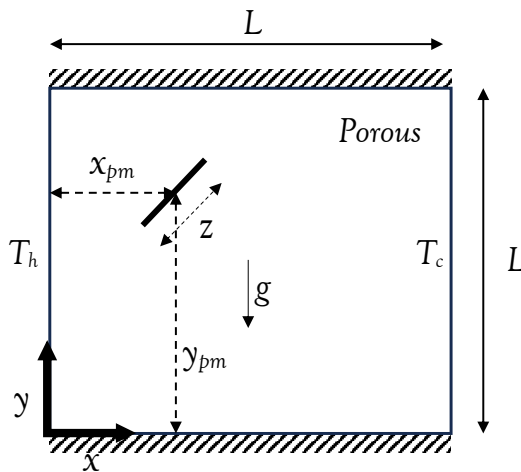


Fig. 1. Schematic diagram of a differentially heated square porous enclosure with a single right-inclined obstruction ( $N = 1$ , type: right-inclined obstruction)

right-inclined obstructions are oriented at  $45^\circ$  with respect to the horizontal. The straight crossed obstruction is a combination of vertical and horizontal obstruction while the inclined-cross obstruction is a combination of left- and right-inclined obstruction.

The flow inside such a porous geometry is represented using Darcy's model along with Boussinesque's approximation in the momentum equation. Let  $v$ ,  $u$ ,  $\mu$ ,  $K$ ,  $p$ ,  $T$ ,  $x$  and  $y$  be the vertical velocity, horizontal velocity, fluid viscosity, permeability of porous medium, pressure, temperature, horizontal and vertical directions, respectively. The conservation equations, as per Darcy's porous flow model are,

$$\frac{\partial u}{\partial x} + \frac{\partial v}{\partial y} = 0 \quad (1)$$

$$u = -\frac{K}{\mu} \left( \frac{\partial p}{\partial x} \right) \quad (2)$$

$$v = -\frac{K}{\mu} \left( \frac{\partial p}{\partial y} + \tilde{\rho} g \right) \quad (3)$$

$$u \frac{\partial T}{\partial x} + v \frac{\partial T}{\partial y} = \alpha_e \left( \frac{\partial^2 T}{\partial x^2} + \frac{\partial^2 T}{\partial y^2} \right) \quad (4)$$

where,

$$\alpha_e = \frac{k_e}{(\rho c_p)_f}$$

$$\tilde{\rho} = \rho_r [1 - \beta(T - T_r)]$$

Here,  $\alpha_e$  and  $n$  are effective thermal diffusivity and unit vector perpendicular to the edges of partition, respectively. These equations are bound by certain conditions, as mentioned below.

	Boundary	Velocity	Temperature
$x = 0$	$0 \leq y \leq L$	$u = 0$	$T = T_h$
$x = L$	$0 \leq y \leq L$	$u = 0$	$T = T_c$
$y = 0, L$	$0 \leq x \leq L$	$v = 0$	$\frac{\partial T}{\partial y} = 0$
$\forall x_p$	$0 \leq y \leq L$	$u, v = 0$	$\frac{\partial T}{\partial n} \Big ^- = \frac{\partial T}{\partial n} \Big ^+$

The above governing equations as well as the boundary conditions are transformed into a dimensionless form by scaling the relevant variables and parameters, as given below,

$$\begin{aligned}
 X &= \frac{x}{L}; & Y &= \frac{y}{L}; & U &= \frac{u}{\alpha_e/L}; & V &= \frac{v}{\alpha_e/L}; \\
 \theta &= \frac{T - T_c}{T_h - T_c}; & Ra &= \frac{Kg\beta(T_h - T_c)L}{\nu\alpha}; & Z &= \frac{z}{L} \\
 X_p &= \frac{x_p}{L}; & Y_p &= \frac{y_p}{L}; & U &= \frac{\partial\psi}{\partial Y}; & V &= -\frac{\partial\psi}{\partial X}.
 \end{aligned} \tag{5}$$

Here,  $Ra$  and  $Z$  denote Darcy-modified Rayleigh number and length of obstruction respectively.  $X$  and  $Y$  are dimensionless horizontal and vertical coordinate axes, respectively, while  $U$  and  $V$  are non-dimensional horizontal and vertical velocities, respectively,  $X_p$  and  $Y_p$  are obstruction specific grid points.  $\psi$  and  $\theta$  are stream function and temperature, respectively. Eq. 1 to Eq. 4 along with boundary condition may be rewritten using the above variables and parameters of Eq. 5 after eliminating pressure from the momentum equations Eq. 2 and Eq. 3, as shown below,

$$\frac{\partial^2\psi}{\partial X^2} + \frac{\partial^2\psi}{\partial Y^2} = -Ra \frac{\partial\theta}{\partial X} \tag{6}$$

$$\frac{\partial\psi}{\partial Y} \frac{\partial\theta}{\partial X} - \frac{\partial\psi}{\partial X} \frac{\partial\theta}{\partial Y} = \frac{\partial^2\theta}{\partial X^2} + \frac{\partial^2\theta}{\partial Y^2} \tag{7}$$

Following are the modified boundary conditions,

	Boundary	Stream function	Temperature
$X = 0$	$0 \leq Y \leq 1$	$\psi = 0$	$\theta = 1$
$X = 1$	$0 \leq Y \leq 1$	$\psi = 0$	$\theta = 0$
$Y = 0, 1$	$0 \leq X \leq 1$	$\psi = 0$	$\frac{\partial\theta}{\partial Y} = 0$
$\forall X_p$	$0 \leq Y \leq 1$	$\psi = 0$	$\frac{\partial\theta}{\partial n} \Big ^- = \frac{\partial\theta}{\partial n} \Big ^+$

The convective rate of heat transfer across the differentially heated square porous enclosure with a trapezoidal partition within it is assessed by evaluating Nusselt number, as given below,

$$Nu_{h,c} = \int_0^{AR} Nu_L dY \tag{8}$$

Here,  $Nu_L$  is the local Nusselt number along the cold and hot wall evaluated as,

$$Nu_L = -\frac{\partial\theta}{\partial X} \Big|_{X=0,1}. \tag{9}$$

### 3. Numerical method

Eqs. 6-7 are coupled partial differential equations. These are transformed into an algebraic form by finite difference method. All the interior nodes are discretized using second-order central difference scheme. Edge-nodes are discretized using second order forward and backward difference. The transformed algebraic form of equations is then solved numerically by Successive Accelerated Replacement Scheme. The specifics of this scheme may be found in [26, 27]. The objective of this scheme is to initialize a profile of required parameter that would satisfy the boundary and partition matching conditions. Let  $\sigma$  be a transport property and  $\tilde{\sigma}_{i,j}^n$  be the error in its governing equation at any particular grid point  $(i, j)$  in  $n^{th}$  iteration. Then,  $(n + 1)^{th}$  approximation of the variable  $\sigma$  is obtained as,

$$(\sigma)_{i,j}^{n+1} = (\sigma)_{i,j}^n - \omega \frac{\tilde{\sigma}_{i,j}^n}{\partial \tilde{\sigma}_{i,j}^n / \partial (\sigma)_{i,j}^n}. \quad (10)$$

Here, the acceleration factor  $\omega$  ranges from 0 to 2 (for the current study, its value is set at 0.7),  $i$  and  $j$  are indices of horizontal and vertical grid point that vary from 1 to  $i_{\max}$  and 1 to  $j_{\max}$ , respectively. In Eq. 10, the denominator of the second term in RHS is the partial derivative of the governing equation relative to its transport property at node  $(i, j)$ . The criteria of convergence for the transport property  $\sigma$  are,

$$\frac{\sum_{i=2}^{i_{\max}-1} \sum_{j=2}^{j_{\max}-1} |(\sigma)_{i,j}^{n+1} - (\sigma)_{i,j}^n|}{\sum_{i=2}^{i_{\max}-1} \sum_{j=2}^{j_{\max}-1} |(\sigma)_{i,j}^{n+1}|} \leq \varepsilon. \quad (11)$$

The strategy for placing a particular obstruction is basically finding the point of maximum absolute stream function in a differentially heated plain porous enclosure (i.e., initially without any obstruction) and subsequently placing a single obstruction at that location. Now, re-running the simulation from the beginning with a single obstruction already embedded, we would get a new location of maximum absolute stream function and subsequently placing a second obstruction at that location. This process goes on until a desirable reduction is achieved.

### 4. Result and discussions

The fluid flow and heat transfer within a differentially heated and cooled of porous enclosure with multiple obstructions are visualized computationally by solving the aforementioned governing equations along with the corresponding boundary conditions. The parameters under study are the various type of obstructions (horizontal, vertical, right-inclined, left-inclined, straight-crossed and inclined-crossed), the number of obstructions ( $0 \leq N \leq 10$ ) and the modified Rayleigh number ( $100 \leq Ra \leq 2000$ ). The size of obstruction ( $Z$ ) has been fixed

at 0.1 as any obstruction smaller than this may not affect the convection strength as such. These configurations of obstructions are individually simulated to visualize the distribution of isotherms, streamlines and the corresponding Nusselt number values.

Initially, a grid sensitivity test is conducted for a differential porous enclosure with the above boundary conditions with no obstructions, as shown in Table 1. The Nusselt number values are evaluated for  $Ra = 100$  and 5000. This would ensure that the solution is coherent with a wide range of Darcy modified Rayleigh number. The grid size is varied from  $25 \times 25$  to  $200 \times 200$  in two-fold increment to ensure the uniformity.

Table 1. Grid sensitivity test. ( $Ra = 100$  and 5000;  $Z = 0$ ;  $N = 0$ )

$Ra$	Grid size	$Nu$	Iterations
100	$25 \times 25$	3.43	88
	$50 \times 50$	3.2	272
	$100 \times 100$	3.11	892
	$200 \times 200$	3.09	2796
5000	$25 \times 25$	23.9	335
	$50 \times 50$	34.96	946
	$100 \times 100$	40.11	2603
	$200 \times 200$	40.26	8114

Considering the computational accuracy (error) and cost (number of iterations), the grid size of  $100 \times 100$  may be accepted for the current investigation. For  $Ra = 100$  and 5000, the Nusselt number for the grid size  $200 \times 200$  is merely 0.64% and 0.37% more precise than that of a grid size  $100 \times 100$ , respectively. Moreover, the number of iterations taken to converge by  $200 \times 200$  mesh is nearly three times greater, which is not justifiable to be chosen. Thus, the analyses conducted hereon are generated with the grid size of  $100 \times 100$ .

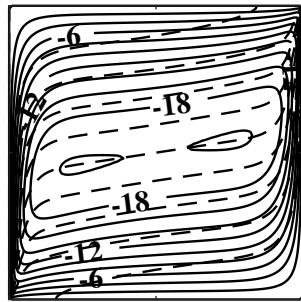
Further, a validation of the computer code for a differentially heated porous enclosure with boundary conditions remaining the same as above, is performed, as shown in Table 2, and the results are compared with the benchmark of those available in literature. The boundary conditions are kept consistent throughout.

Table 2. Validation of code for porous enclosure without partition. ( $Ra = 10$ , 100 and 1000;  $Z = 0$ ;  $N = 0$ )

$Ra$	$Nu$ (Present)	[28]	[29]	[30]	[31]
10	1.079	–	–	1.079	1.080
100	3.11	4.2	3.141	3.16	3.27
1000	15.78	15.8	13.448	14.06	18.27

The above grid test and validation of differentially heated porous enclosure has assured the credibility of the applied computer program and consequently has been used with greater certainty to solve the problem mentioned in previous section.

Fig. 2 shows streamlines (solid lines) and isotherms (dashed lines) for porous enclosure without any obstruction for the modified Rayleigh number  $Ra$  of 1000, length  $Z$  and the number of obstructions  $N$  equal to zero. These contours would serve as a reference to understand the effect of obstructions inserted within this differentially heated porous enclosure. It should be noted that there is a big stagnant streamline around the center of the enclosure that signifies the strength of convection flow developed within it. Further, the isotherms (dashed line) can be seen to rise sharply from hot left wall, travel towards the right wall and again climb sharply on the cold right wall. The maximum absolute value of stream function is 20.06 and the Nusselt number is 15.78. The location of maximum absolute stream function is 0.76 along horizontal direction and 0.54 along vertical direction. The total non-dimensional length of square porous enclosure equal to one in horizontal as well as vertical direction.



$$Nu = 15.78; |\psi|_{\max} = 20.06$$

Fig. 2. Streamlines (solid lines) and isotherms (dashed lines) for porous enclosure without any obstruction ( $Ra = 1000$ ,  $Z = 0$ ,  $N = 0$ )

#### 4.1. Effect of horizontal obstruction

Fig. 3 shows streamlines (solid lines) and isotherms (dashed lines) for selectively positioned horizontal diathermal obstructions within the porous enclosure for a modified Rayleigh number  $Ra$  of 1000, length  $Z$  of 0.1 and the number of obstructions  $N$  increasing from 1 to 4. The number of obstructions may be as high as possible. However, four obstructions are sufficient to occupy the entire space of the enclosure. As the  $(X, Y)$  location of maximum absolute stream function is  $(0.76, 0.54)$ , as mentioned previously and shown in Table 3, a single horizontal obstruction of length  $Z$  0.1 is inserted at this location. Upon re-running the simulation, a slight change is found in streamlines and temperature distribution, as shown



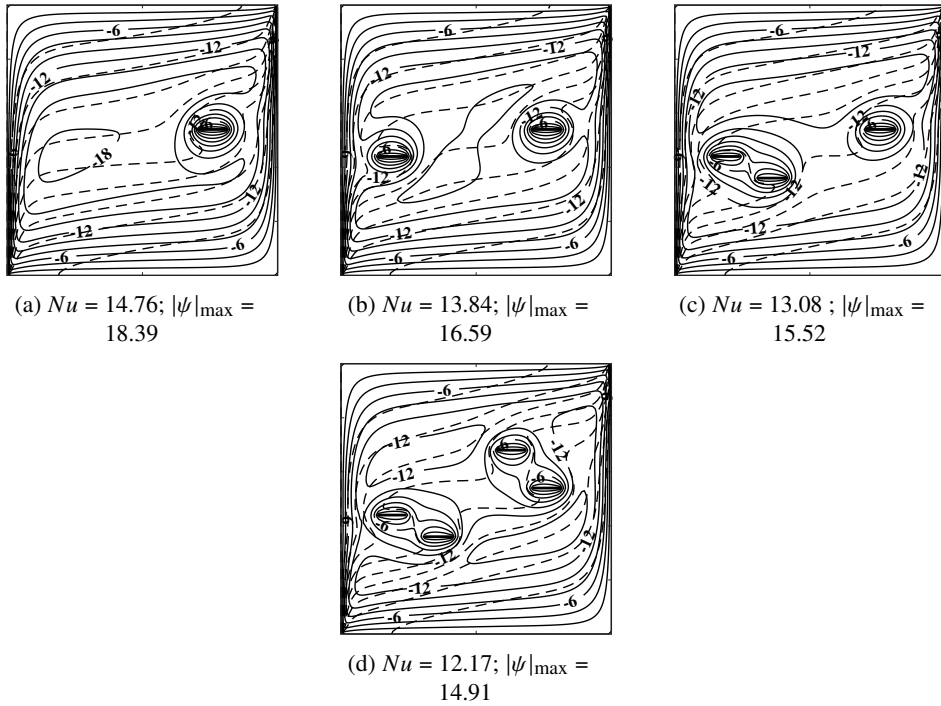


Fig. 3. Streamlines (solid lines) and isotherms (dashed lines) for selectively positioned horizontal diathermal obstructions within porous enclosure ( $Ra = 1000$ ,  $Z = 0.1$ ,  $N = 1$  to 4)

in Fig. 3a. The value of maximum absolute stream function and Nusselt number is 18.39 and 14.76, respectively, which means a decrease by 8.3% and 6.46%, respectively. The new updated location of maximum absolute stream function is (0.19, 0.44), as shown in Table 3.

Table 3. Position of obstructions. (type - horizontal,  $Ra = 1000$ ,  $N = 1$  to 4,  $L = 0.1$ )

Obstruction	$X_{pm}$	$Y_{pm}$
1	0.76	0.54
2	0.19	0.44
3	0.36	0.36
4	0.63	0.68

Inserting another horizontal obstruction of same length  $Z$  of 0.1 at this location and re-running the simulation, we get streamlines and temperature distribution as shown in Fig. 3b where a slight change can be seen again. The value of maximum absolute stream function and the Nusselt number decrease by 17.3% and 12.29%, respectively, which is a significant drop. The new updated location of maximum absolute stream function is (0.36, 0.36), as shown in Table 3. Inserting

a third horizontal obstruction at this location as shown in Fig. 3c, and re-running the simulation, we get a reduction of 22.63% and 17.11% in maximum absolute stream function and the Nusselt number, respectively, which again is a substantial reduction. The new updated location of  $|\psi|_{\max}$  is (0.63,0.68), as shown in Table 3. The fourth horizontal obstruction at this location, as shown in Fig. 3d, reduces the maximum absolute stream function and the Nusselt number value by 25.67% and 22.88%, respectively. At this point, it may be noted that the total net length of inserted obstruction is 0.4 only, which is even less than a half of the characteristic length of the entire porous enclosure, and the reduction in convection heat transfer rate achieved is almost 23%. The reason for such a substantial reduction with fewer obstructions is the weakening of convection flow where it is the strongest, i.e., at the point of maximum absolute stream function, since an obstruction is inserted at exactly this location. The embedded obstructions act as flow blockage or deviator which weakens the nucleus of the flow regime, which subsequently weakens the convection flow and thus the rate of heat transfer.

#### 4.2. Effect of vertical obstruction

Fig. 4 illustrates streamlines (solid lines) and isotherms (dashed lines) for selectively positioned vertical diathermal obstructions within the porous enclosure for a modified Rayleigh number  $Ra$  of 1000, length  $Z$  of 0.1 and the number of obstructions  $N$  from 1 to 4.

A single vertical obstruction of length  $Z$  0.1 is inserted at (0.76, 0.54) which is the location of maximum absolute stream function for the porous enclosure without any obstruction, as mentioned previously and shown in Table 4. Repeating the strategy mentioned in section (4.1), we obtain the streamlines and temperature distribution for single vertical obstruction, as shown in Fig. 4a, where the maximum absolute stream function and Nusselt number is seen to drop by 8.87% and 6.65%, respectively. This drop is marginally better than that caused by horizontal obstruction. The new updated location of maximum absolute stream function is (0.19, 0.44), as shown in Table 4. This location is same as that for the second horizontal obstruction. Inserting the second vertical obstruction at this location, as shown in Fig. 4b, reduces the maximum absolute stream function and the Nusselt number by 18.54% and 12.67%, respectively, which is a significant drop and again is marginally better than that caused by the second horizontal obstruction. The new updated location of maximum absolute stream function is (0.34, 0.34), as shown in Table 4, and quite near to that of the third horizontal obstruction. Inserting the third vertical obstruction at this location, as shown in Fig. 4c, gives a reduction of 22.68% and 17.81% in maximum absolute stream function and the Nusselt number, respectively, which again is a substantial reduction and is a slightly better than the reduction caused by its counterpart, i.e., the horizontal obstruction. The new updated location of  $|\psi|_{\max}$  is (0.65,0.69), as shown in Table 4. A fourth vertical obstruction at this location, as shown in Fig. 4d, reduces the maximum absolute stream function

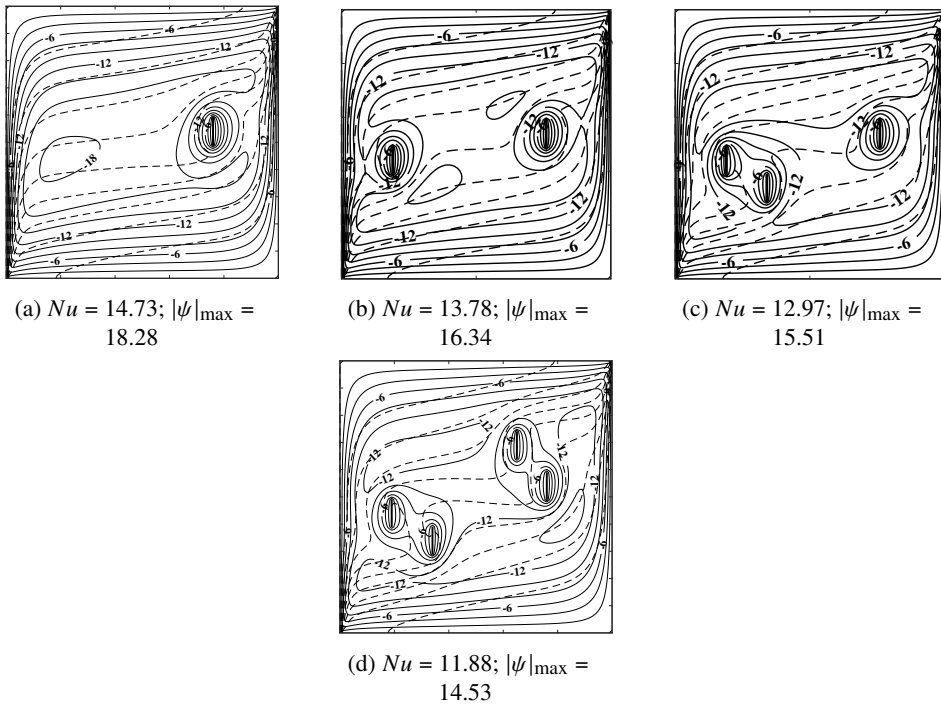


Fig. 4. Streamlines (solid lines) and isotherms (dashed lines) for selectively positioned vertical diathermal obstructions within porous enclosure ( $Ra = 1000$ ,  $Z = 0.1$ ,  $N = 1$  to 4)

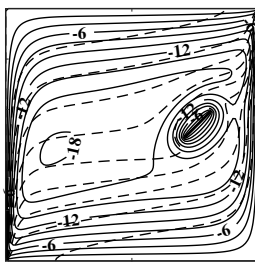
Table 4. Position of obstructions. (*type* - vertical,  $Ra = 1000$ ,  $N = 1$  to 4,  $L = 0.1$ )

Obstruction	$X_{pm}$	$Y_{pm}$
1	0.76	0.54
2	0.19	0.44
3	0.34	0.34
4	0.65	0.69

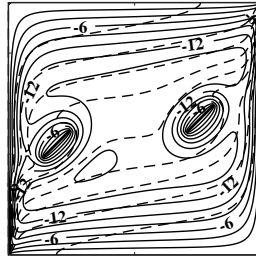
and the Nusselt number value by 27.57% and 24.71%, respectively. Since the fluid flowing towards the right wall encounters a vertical obstruction which is almost perpendicular to its direction, a marginally greater reduction is seen in this case as compared to that of horizontal direction. Also, in literature, a full vertical partition showed better reduction than its horizontal counterpart. The advantage of the current strategy presented here is that with an effective length of only 0.4, a reduction in convection heat transfer is about 25% which is at par with that of full vertical partition. Thus, instead of inserting a full partition, only a couple of obstruction when strategically inserted at right locations would bring about the similar effect. The objective of the current study is thus fulfilled. The thermal designers would be able to use the available space in porous enclosures more efficiently using this strategy.

### 4.3. Effect of right-inclined obstruction

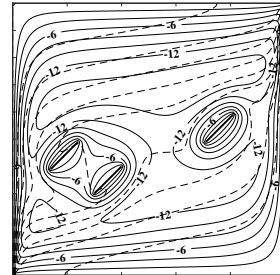
Fig. 5 shows streamlines (solid lines) and isotherms (dashed lines) for selectively positioned right-inclined diathermal obstructions within a porous enclosure for the modified Rayleigh number  $Ra$  of 1000, length ( $Z$ ) of 0.1 and the number of obstructions  $N$  from 1 to 4. Similar to previous cases, a single right-inclined obstruction of length ( $Z$ ) 0.1 inserted at (0.76, 0.54) develops streamlines and temperature distribution as shown in Fig. 5a. As can be seen, the maximum absolute stream function and the Nusselt number drop by 9.42% and 7.67%, respectively. This drop is marginally better than that caused by vertical as well as horizontal obstructions.



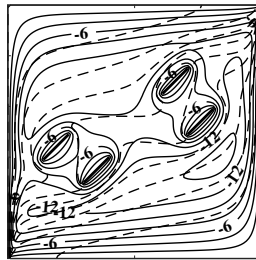
(a)  $Nu = 14.57$ ;  $|\psi|_{\max} = 18.17$



(b)  $Nu = 13.53$ ;  $|\psi|_{\max} = 16.23$



(c)  $Nu = 12.64$ ;  $|\psi|_{\max} = 15.13$



(d)  $Nu = 11.50$ ;  $|\psi|_{\max} = 14.51$

Fig. 5. Streamlines (solid lines) and isotherms (dashed lines) for selectively positioned right inclined diathermal obstructions within porous enclosure ( $Ra = 1000$ ,  $Z = 0.1$ ,  $N = 1$  to 4)

The reason behind this may be attributed to the fact that the inclined obstruction inherits the advantage of both vertical and horizontal geometry, in a sense that a typical fluid flowing towards such inclined obstruction is obstructed along vertical direction as well as horizontal directions thus leaving the flow strength slightly more weakened. The location of the second obstruction comes out to be same as that of the second vertical and horizontal obstruction, i.e., (0.19, 0.44), as shown in Table 5 and Fig. 5b. A drop of 19.09% and 14.26% is seen in the maximum absolute

Table 5. Position of obstructions. (*type* – right-inclined,  
 $Ra = 1000$ ,  $N = 1$  to 4,  $L = 0.1$ )

Obstruction	$X_{pm}$	$Y_{pm}$
1	0.76	0.54
2	0.19	0.44
3	0.35	0.35
4	0.66	0.7

stream function and the Nusselt number, respectively, which is a significant drop and again a better reduction than that caused by the second horizontal as well as vertical obstructions. The third location is (0.35, 0.35), as shown in Table 5 and Fig. 5c, which is almost the same as the third horizontal and vertical obstructions. It brings about a reduction of 24.58% and 19.09% in the maximum absolute stream function and the Nusselt number, respectively, which again is a significant reduction and a relatively better reduction than that of its previous counterpart, i.e., horizontal and vertical obstruction. In a similar fashion, the fourth right-inclined obstruction at (0.66, 0.7), as shown in Table 5 and Fig. 5d, brings about a decrease of 27.67% and 27.12% in the maximum absolute stream function and the Nusselt number, respectively. Again, with net effect obstruction length of 0.4, the convection strength is curtailed by 27% which is significant enough.

#### 4.4. Effect of left-inclined obstruction

Fig. 6 shows streamlines (solid lines) and isotherms (dashed lines) for selectively positioned left-inclined diathermal obstructions within a porous enclosure for the modified Rayleigh number  $Ra$  of 1000, length ( $Z$ ) of 0.1 and the number of obstructions  $N$  from 1 to 4. Similar to previous cases, a single, double, triple and quadruple left-inclined obstruction of length ( $Z$ ) 0.1 inserted sequentially and strategically would produce a drop of 9.52%, 19.44%, 25.77%, 28.96% in the stream function and 8.05%, 15.15%, 20.85%, 28.14% in the Nusselt number, respectively. These results are much better than previously obtained with horizontal and vertical obstructions while marginally better than those of right-inclined obstructions, since geometrically these are quite similar. Also, the locations of these four obstructions are almost the same as in all previous cases, as seen from Table 6.

Although marginally, but left-inclined obstruction performs better than the right-inclined one due to the nature of boundary conditions. The temperature gradients in Fig. 2 can be seen extremely crowded near the bottom left corner and top right corner of the porous enclosure. This indicates that these are the hotspots of convection strength. Keeping this in mind, we conclude that the geometry of left-inclined obstruction is such that it tries to shield these two corner hotspot zones attaining a direction perpendicular to them. This can also be noticed by carefully inspecting the streamline direction in the interior portion of enclosure of Fig. 6

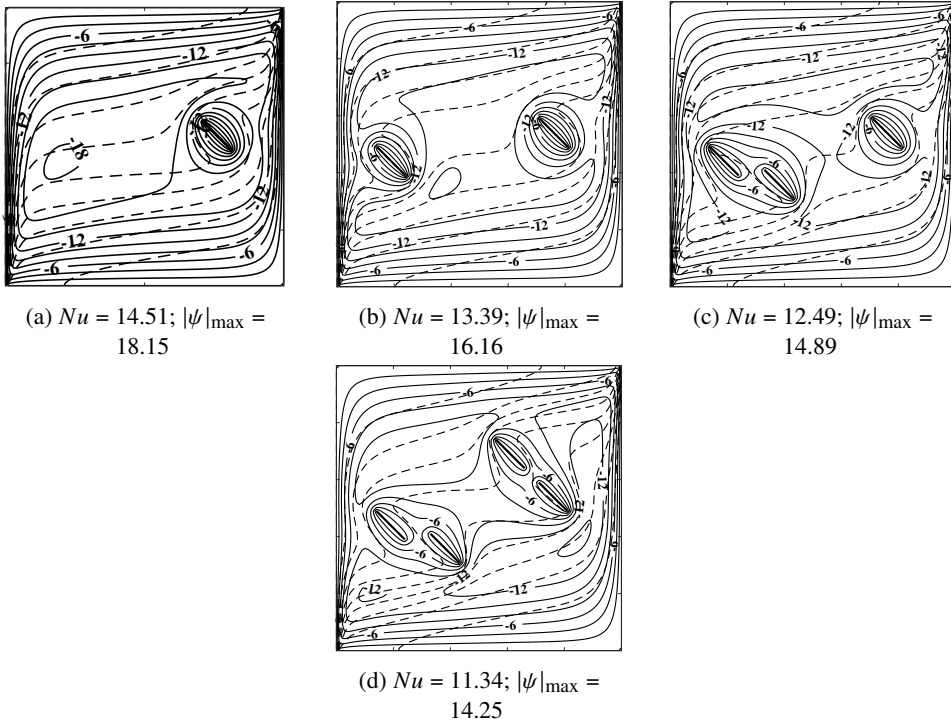


Fig. 6. Streamlines (solid lines) and isotherms (dashed lines) for selectively positioned left inclined diathermal obstructions within porous enclosure ( $Ra = 1000$ ,  $Z = 0.1$ ,  $N = 1$  to 4)

Table 6. Position of obstructions. (*type* – left-inclined,  $Ra = 1000$ ,  $N = 1$  to 4,  $L = 0.1$ )

Obstruction	$X_{pm}$	$Y_{pm}$
1	0.76	0.54
2	0.19	0.44
3	0.38	0.36
4	0.61	0.69

which is horizontal and slightly raised towards its right side. This flow is obstructed in approximately perpendicular direction by the left-inclined obstructions thus leaving a greater effect on the flow strength as compared to its previous counterparts viz., horizontal, vertical and right-inclined partition.

#### 4.5. Effect of straight-crossed obstruction

Fig. 7 shows streamlines (solid lines) and isotherms (dashed lines) for selectively positioned straight-crossed diathermal obstructions within the porous enclosure for the modified Rayleigh number  $Ra$  of 1000, length ( $Z$ ) of 0.1 and the number of obstructions  $N$  from 1 to 4.

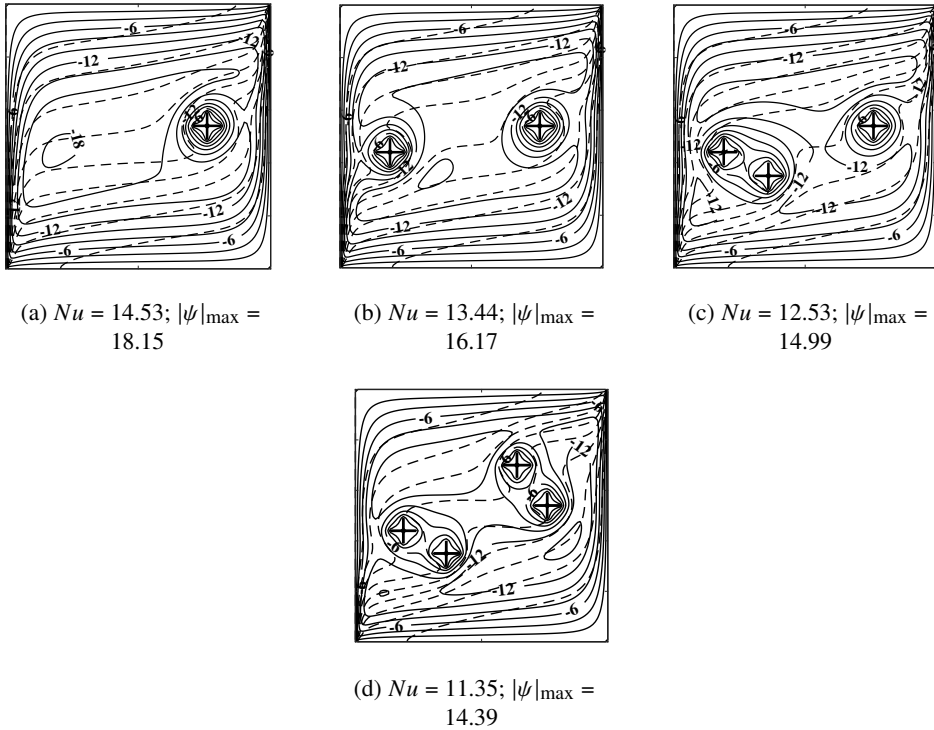


Fig. 7. Streamlines (solid lines) and isotherms (dashed lines) for selectively positioned straight-crossed diathermal obstructions within porous enclosure ( $Ra = 1000$ ,  $Z = 0.1$ ,  $N = 1$  to 4)

Here, vertical and horizontal obstructions are involved concurrently and thus are expected to yield a better reduction than each of them compared individually. From Fig. 7 it is clear that the reduction obtained in maximum absolute stream function is about 9.52%, 19.39%, 25.27%, 28.27% and for the Nusselt number it is about 7.92%, 14.83%, 20.60%, 28.07% for single, double, triple and quadruple straight-crossed obstructions respectively. These results are better than those for horizontal and vertical obstructions. For a total of four obstructions, the Nusselt number for the straight-crossed obstruction case shows a drop 4.46% greater than for the vertical obstruction case while a drop 6.75% greater than for the horizontal obstruction case. The locations of these four obstructions are almost the same as

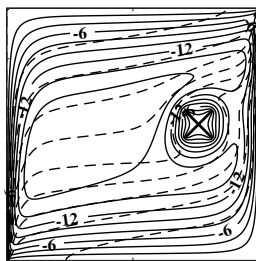
Table 7. Position of obstructions. (*type* – straight-crossed,  $Ra = 1000$ ,  $N = 1$  to 4,  $L = 0.1$ )

Obstruction	$X_{pm}$	$Y_{pm}$
1	0.76	0.54
2	0.19	0.44
3	0.36	0.35
4	0.64	0.7

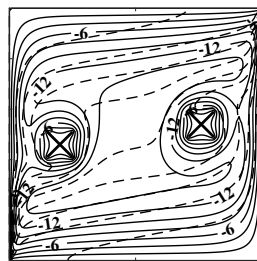
in all previous cases, as seen from Table 7. It may also be noted that left-inclined obstructions still produce marginally better or almost the same reduction in the strength of convection heat transfer.

#### 4.6. Effect of inclined-crossed obstruction

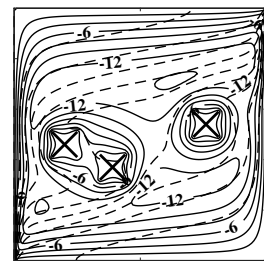
Fig. 8 shows streamlines (solid lines) and isotherms (dashed lines) for selectively positioned straight-crossed diathermal obstructions within the porous enclosure for the modified Rayleigh number  $Ra$  of 1000, length ( $Z$ ) of 0.1 and the number of obstructions  $N$  from 1 to 4.



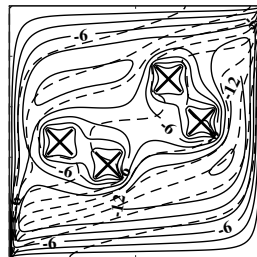
(a)  $Nu = 14.24$ ;  $|\psi|_{\max} = 17.94$



(b)  $Nu = 12.98$ ;  $|\psi|_{\max} = 15.95$



(c)  $Nu = 11.96$ ;  $|\psi|_{\max} = 14.15$



(d)  $Nu = 10.64$ ;  $|\psi|_{\max} = 14.09$

Fig. 8. Streamlines (solid lines) and isotherms (dashed lines) for selectively positioned inclined-crossed diathermal obstructions within porous enclosure ( $Ra = 1000$ ,  $Z = 0.1$ ,  $N = 1$  to 4)

Here, the left-inclined and right-inclined obstructions are both involved concurrently and thus expected to yield a better reduction than each of them compared individually. From Fig. 8 it is evident that for single, double, triple and quadruple inclined-crossed obstructions the reduction obtained in maximum absolute stream function is about 10.57%, 20.49%, 29.46%, 29.76% and for the Nusselt number is about 9.76%, 17.74%, 24.21%, 32.57%, respectively. These results are comparatively better than those of left-inclined and right-inclined obstructions. For a total of four obstructions, the Nusselt number for the inclined-crossed obstruction case



generates 7.48% greater drop than for the right-inclined obstruction case while 6.17% drop more than left-inclined obstruction case. The locations of these four obstructions are almost the same as in all previous cases as seen from Table 8. It may also be noted that, relative to straight-crossed obstruction case, the inclined-crossed obstruction still performs better by producing a drop in Nusselt number of about 6.26% greater than the previous one.

Table 8. Position of obstructions. (*type* – inclined-crossed,  $Ra = 1000$ ,  $N = 1$  to 4,  $L = 0.1$ )

Obstruction	$X_{pm}$	$Y_{pm}$
1	0.76	0.54
2	0.2	0.46
3	0.39	0.37
4	0.63	0.71

#### 4.7. Effect of modified Rayleigh number

A common similarity in all the previous cases is the location of obstructions. All the obstructions from the first to fourth one, had almost the same location. One of the reasons for that may be attributed to the fluid and porous properties which are characterized by the modified Rayleigh number. In this section, the effect of the modified Rayleigh number on natural convection heat transfer within a differentially heated porous enclosure is investigated for various types of obstructions under study. A total of four obstructions of all types are embedded.

Fig. 9 illustrates streamlines (solid lines) and isotherms (dashed lines) for selectively positioned four horizontal diathermal obstructions within a differentially heated porous enclosure for different values of Rayleigh number  $Ra$  viz., 100, 500, 1000, 2000 and length  $Z$  of 0.1. As can be seen clearly, the locations of obstructions change with every value of the modified Rayleigh number. The locations are:

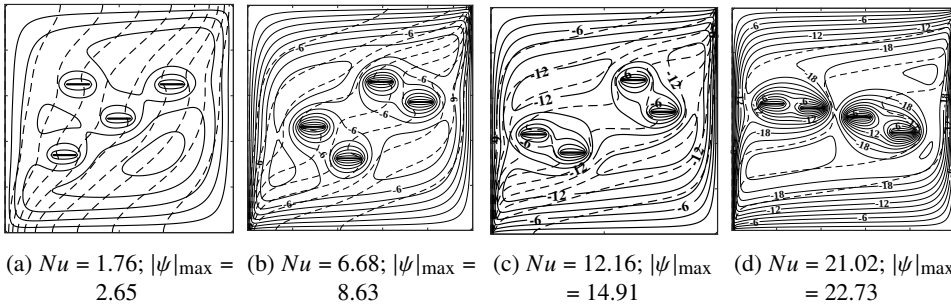


Fig. 9. Streamlines (solid lines) and isotherms (dashed lines) for selectively positioned horizontal diathermal obstructions within porous enclosure for varying Rayleigh number ( $Ra = 100, 500, 1000, 2000$ ;  $Z = 0.1$ ;  $N = 4$ )

(0.5,0.5), (0.73, 0.65), (0.26, 0.34) and (0.32, 0.65) for  $Ra$  value of 100, as seen in Fig. 9a. For smaller values of  $Rs$ , the obstructions are seen to be approximately aligned along the diagonal of the square enclosure. It is to be noted that this diagonal path is from bottom-left corner to top-right corner. As stated in section 4.4, these are the hotspots for the strength of convective natural convection developed within the enclosure. These obstructions tend to form a clear disturbance in between these hotspots to deviate the flow away from its usual path, thus effectively weaken the convection flow. For the higher value of  $Ra$  (2000), however, the obstructions are aligned along the central horizontal region at (0.57, 0.51), (0.77,0.44), (0.36,0.55) and (0.18,0.57), since for the higher Rayleigh number the convection strength is greater and the flow tends to move swiftly along vertical directions. In Fig. 9d the obstruction can be seen to form a barricade for this vertical flow which hampers the flow much more effectively. Thus, the strategy adopted in the current study seems to be adaptable for a wide range of Rayleigh numbers and seems to be more effective than the fully partitioned approach.

Fig. 10 illustrates streamlines (solid lines) and isotherms (dashed lines) for selectively positioned four vertical diathermal obstructions within a differentially heated porous enclosure for different values of Rayleigh number  $Ra$  viz., 100, 500, 1000, 2000 and length  $Z$  0.1. As it can be seen clearly again, the locations of obstructions change in a similar fashion with every value of the modified Rayleigh number. Even in this case, the strategy that is deployed tends to align the obstructions in such a manner so that the flow is obstructed in its strongest region, and consequently a shield is formed between the differentially heated walls based on the flow pattern. A slight nuance may be seen in the alignment of obstructions in Fig. 9b and Fig. 10b, which is for the Rayleigh number of 500. The locations are (0.29,0.46), (0.77,0.57), (0.59,0.66) and (0.45,0.32) for horizontal obstructions while (0.29,0.46), (0.77,0.57), (0.46, 0.35) and (0.19,0.6) for vertical obstructions. The first and the second obstructions seem to be situated at identical locations, but

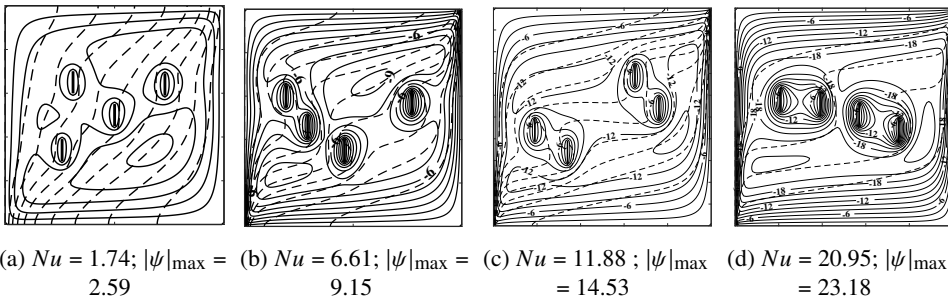


Fig. 10. Streamlines (solid lines) and isotherms (dashed lines) for selectively positioned vertical diathermal obstructions within porous enclosure for varying Rayleigh number ( $Ra = 100, 500, 1000, 2000$ ;  $Z = 0.1$ ;  $N = 4$ )

the difference appears in the third and fourth obstructions. This may be due the vertical orientation of obstruction (in this case, the hindrance is along the flow). Since the flow is also in vertical direction (due to convection), the hindrance created by vertical obstruction is entirely different then that caused by horizontal obstruction (in this case, the hindrance is directly perpendicular to the flow).

Fig. 11 and Fig. 12 illustrate streamlines (solid lines) and isotherms (dashed lines) for selectively positioned four right-inclined and left-inclined diathermal obstructions, respectively within a differentially heated porous enclosure for different values of Rayleigh number  $Ra$  viz., 100, 500, 1000, 2000 and length  $Z$  of 0.1. It is clearly evident that, the location of obstructions change according to the value of modified Rayleigh number. Also, the locations for each case are quite similar for both types of obstructions. Again, in these cases also the locations slightly differ for  $Ra$  500.

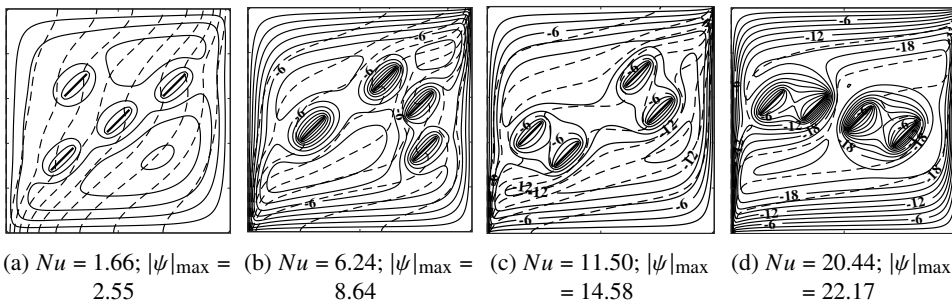


Fig. 11. Streamlines (solid lines) and isotherms (dashed lines) for selectively positioned right-inclined diathermal obstructions within porous enclosure for varying Rayleigh number ( $Ra = 100, 500, 1000, 2000$ ;  $Z = 0.1$ ;  $N = 4$ )

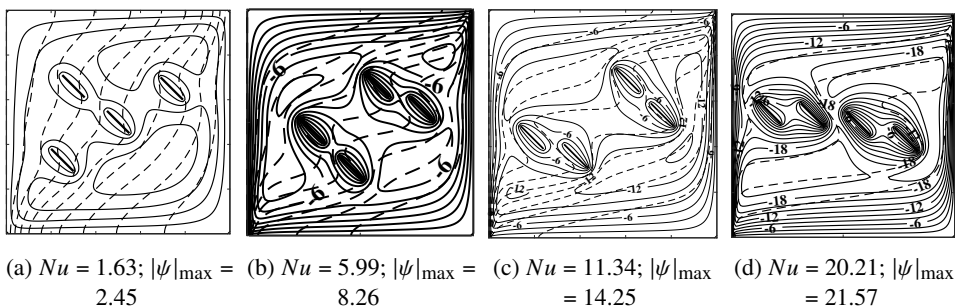


Fig. 12. Streamlines (solid lines) and isotherms (dashed lines) for selectively positioned left-inclined diathermal obstructions within porous enclosure for varying Rayleigh number ( $Ra = 100, 500, 1000, 2000$ ;  $Z = 0.1$ ;  $N = 4$ )

This may be attributed to the convection hotspots located at the bottom-left corner and the top-right corner as mentioned previously in section 4.4. The isotherms can be seen to move along this diagonal direction. The right-inclined obstruction is

aligned along this direction, while the left-inclined one is aligned perpendicular to this diagonal direction. Further, the Rayleigh number of 500 is neither very weak nor very strong in terms of convection strength.

Fig. 13 and Fig. 14 illustrate streamlines (solid lines) and isotherms (dashed lines) for selectively positioned four straight-crossed and inclined-crossed diathermal obstructions, respectively, within a differentially heated porous enclosure for different values of Rayleigh number  $Ra$  viz., 100, 500, 1000, 2000 and length  $Z$  of 0.1. Here, the alignment of obstructions seems to be quite similar to its individual type counterparts. That is to say, the straight-crossed obstruction alignments are quite similar to those of horizontal/vertical obstructions while the inclined-crossed obstruction alignments are quite similar to those of right-inclined/left-inclined obstructions. This is expected since the nature of geometry is similar. An overall view of the drop of convection heat transfer reveals that a strong reduction may be obtained both for the lower as well as the higher Rayleigh number values. This effect may be better understood by observing the details in Fig. 15.

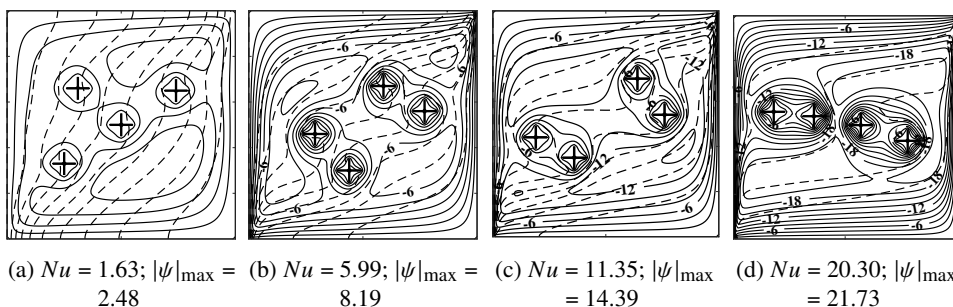


Fig. 13. Streamlines (solid lines) and isotherms (dashed lines) for selectively positioned straight-crossed diathermal obstructions within porous enclosure for varying Rayleigh number ( $Ra = 100, 500, 1000, 2000$ ;  $Z = 0.1$ ;  $N = 4$ )

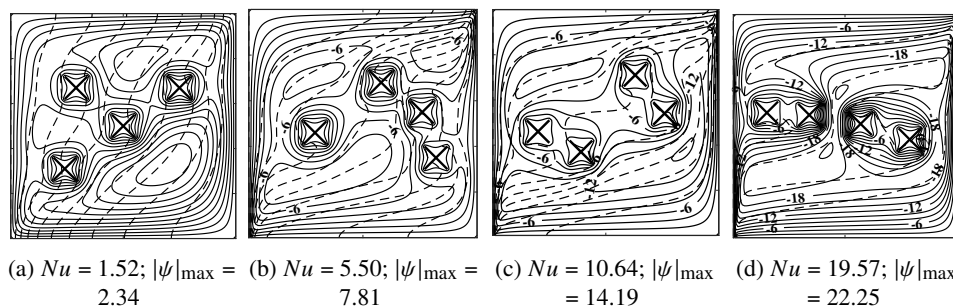


Fig. 14. Streamlines (solid lines) and isotherms (dashed lines) for selectively positioned inclined-crossed diathermal obstructions within porous enclosure for varying Rayleigh number ( $Ra = 100, 500, 1000, 2000$ ;  $Z = 0.1$ ;  $N = 4$ )

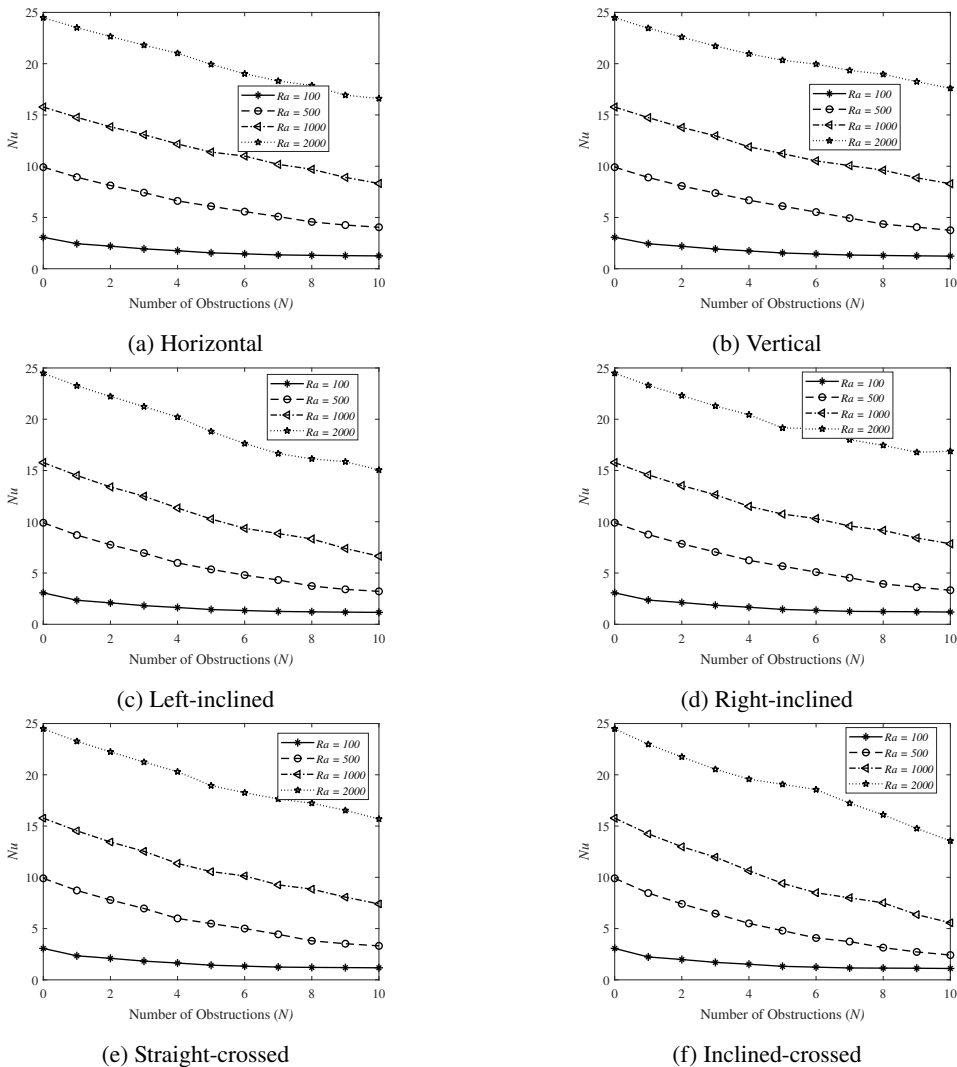


Fig. 15. Effect of number of obstructions ( $N$ ) on Nusselt number ( $Nu$ ) for different type of obstructions at various Rayleigh numbers ( $Ra = 100, 500, 1000, 2000; Z = 0.1; N = 0$  to  $10$ )

The above discussion summarizes and depicts the effect of number of obstructions ( $N = 0$  to  $10$ ) of length ( $Z$ )  $0.1$  on the Nusselt number ( $Nu$ ) for all types of obstructions at various Rayleigh numbers ( $Ra = 100, 500, 1000, 2000$ ) within a porous enclosure. In the above discussion, the number of obstructions was restricted to four due to space constraints assumed in the article. However, the effect of increased number of obstructions may be comprehended from Fig. 15 where the number of obstructions varies from  $0$  to  $10$ . Here,  $N = 0$  denotes a porous enclosure without any obstruction and the maximum number is limited to  $10$  since the total

effective length then becomes 1 (since  $Z = 0.1$ ), which is the characteristic length of the square enclosure.

A clear evidence of decreasing trend in Nusselt number values can be seen as the number of obstruction increases. This is expected due to the fact that as  $N$  increases, the obstruction to flow increases, convection strength weakens and thus the Nusselt number drops. The drop in Nusselt number from no obstruction to 10 obstructions for the Rayleigh number of 100 is 59.14%, 59.8%, 61.05%, 62.08%, 61.65% and 63.82%, while that for the Rayleigh number 2000 is 29.33%, 33.52%, 32.66%, 40.56%, 37.87% and 47.57% for horizontal, vertical, right-inclined, left-inclined, straight-crossed and inclined-cross obstruction types, respectively. The same trend has been presented in previous discussion, as well. Thus, the effect of the number of obstructions is more pronounced in the case of lower Rayleigh number as compared to the higher one, since the lower Rayleigh number already causes that convection flow is not very strong. Addition of obstructions is then more effective in the already weakened convection fluid flow. Achieving such a high reduction in convection heat transfer would certainly help thermal design engineers to improve the effectiveness of porous insulation which is inherently subjected to differential heating.

The above comparison can be clearly seen over a wide range of Rayleigh number in Fig. 16 which is plotted to compare all types of obstructions within a porous enclosure with respect to the Rayleigh number ( $Ra$ ) ( $Ra$  varying from 200 to 2000 with the length  $Z$  of 0.1 and the number of obstructions  $N$  equal to four). A clear rise in the Nusselt number with the increase of the Rayleigh number can be seen. Further, the zoomed-in view of a part of the graph also shows that irrespective of the Rayleigh number value, the inclined-cross obstacle is invariably

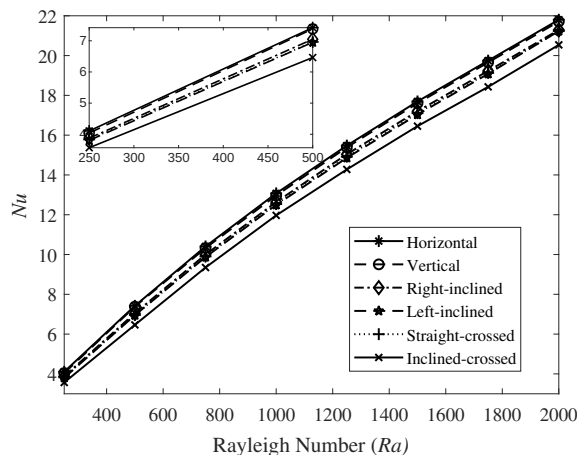


Fig. 16. Comparison of different types of obstructions with respect to Rayleigh number ( $Ra$ ) within porous enclosure ( $Ra = 200$  to  $2000$ ;  $Z = 0.1$ ;  $N = 4$ )

the most effective one that significantly brings down the Nusselt number value. Apart from that, the curves for horizontal and vertical obstruction are very close to each other, while the vertical obstruction curve marginally below the horizontal obstruction curve. Further, the right-inclined, left-inclined and straight crossed obstruction curves are very close to each other, while the left-inclined obstruction shows a comparatively better reduction amongst the three ones.

Another comparison between all types of partitions is shown in Fig. 17 which compares these obstructions within a porous enclosure with respect to the number of obstructions ( $N$ ) varying from 0 to 10, for the Rayleigh number ( $Ra$ ) 1000 and the length ( $Z$ ) 0.1. Yet again, it is evident that irrespective of the number of obstructions embedded within the differentially heated porous enclosure, the inclined-cross obstruction yields a better reduction in the Nusselt number than other types. Also, the rise in the number of obstructions tends to reduce the Nusselt number value.

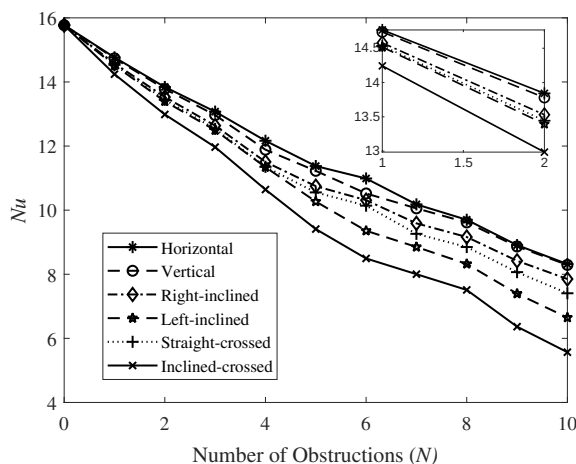


Fig. 17. Comparison of different types of obstructions with respect to number of obstructions ( $N$ ) within porous enclosure ( $Ra = 1000$ ;  $Z = 0.1$ ;  $N = 0$  to 10)

## 5. Conclusions

The current investigation is aimed at reducing the convection heat transfer across a differentially heated porous enclosure by introducing various types of obstructions that are sequentially and strategically placed within the enclosure. The parameters under study are type of obstructions (horizontal, vertical, right-inclined, left-inclined, straight-crossed and inclined-crossed), the number of obstructions ( $0 \leq N \leq 10$ ) and the modified Rayleigh number ( $100 \leq Ra \leq 2000$ ). The size of obstruction ( $Z$ ) has been fixed at 0.1. The Darcy flow model is solved using Successive Accelerated Replacement scheme using the finite difference method.

Isotherms and streamlines are plotted to see the effect of obstructions on convection strength. Finally, the Nusselt number is evaluated to quantify the rate of convection heat transfer. The following conclusions may be drawn from the above discussion:

1. Introducing obstructions within a differentially heated porous enclosure weakens the convection strength developed within it.
2. The increasing order of effective reduction in the Nusselt number according to obstruction type is: horizontal, vertical, right-inclined, straight-crossed, left-inclined and inclined-crossed (considering the higher and the lower Rayleigh number, the obtained average reduction is 44.23%, 46.66%, 46.85%, 49.76%, 51.32% and 55.69%, respectively, with the length of each of the 10 obstructions being 10% of the total characteristic length of enclosure).
3. Reduction in Nusselt number by horizontal and vertical obstructions are quite similar with marginally better reduction by vertical obstructions.
4. Reduction in Nusselt number by right-inclined and left-inclined obstructions is quite similar with marginally better reduction by left-inclined obstructions.
5. Inclined-cross type of obstructions yield maximum reduction in convection strength irrespective of the number of partitions or Rayleigh number.
6. Enclosures with a lower Rayleigh number are more sensitive to obstructions as compared to those with a higher Rayleigh number, i.e., higher drop in Nusselt number is achieved for the lower  $Ra$  values than with the higher ones (considering all types of obstructions, the average reduction in Nusselt number from no obstruction to 10 obstructions is about 61.26% for the lower Rayleigh number while for higher Rayleigh number the reduction is 36.92%).

In the present investigation, we have developed a novel strategy to reduce the convection heat transfer across a differentially heated, fluid-saturated porous enclosure. It is recommended to use inclined-crossed type of obstruction to achieve maximum reduction in the strength of convective flow. The study may be further extended to comprehend the effect size of obstructions in terms of length and thickness, i.e., a conjugate analysis may be done. The usage of curved obstructions like circular, sinusoidal, elliptical and corrugated ones may be a limitation for the approach used in this paper. However, the study of curved obstruction using finite element method, finite volume method may produce interesting results.

## References

- [1] D.B. Ingham, A. Bejan, E. Mamut, and I. Pop. *Emerging Technologies and Techniques in Porous Media*. Springer, 2012. doi: [10.1007/978-94-007-0971-3](https://doi.org/10.1007/978-94-007-0971-3)
- [2] K. Vafai and H. Hadim. Overview of current computational studies of heat transfer in porous media and their applications-natural and mixed convection. In W.J. Minkowych (ed.) *Advances in Numerical Heat Transfer*, volume 2, chapter 10, pages 331–369, Taylor & Francis Group, 2019. doi: [10.1201/9781315136882](https://doi.org/10.1201/9781315136882).



- [3] R. Vadi and K. Sepanloo. An improved porous media model for nuclear reactor analysis. *Nuclear Science and Techniques*, 27:24, 2016. doi: [10.1007/s41365-016-0016-7](https://doi.org/10.1007/s41365-016-0016-7).
- [4] M.A.B. Zanoni, J. Wang, J.L. Torero, and J.I. Gerhard. Multiphase modelling of water evaporation and condensation in an air-heated porous medium. *Applied Thermal Engineering*, 212:118516, 2022. doi: [10.1016/j.applthermaleng.2022.118516](https://doi.org/10.1016/j.applthermaleng.2022.118516).
- [5] A. Chakravarty, K. Ghosh, S. Sen, and A. Mukhopadhyay. Impact of liquid coolant subcooling on boiling heat transfer and dryout in heat-generating porous media. *Thermal Science and Engineering Progress*, 30:101251, 2022. doi: [10.1016/j.tsep.2022.101251](https://doi.org/10.1016/j.tsep.2022.101251).
- [6] G.R. Shanker and K.O. Homan. Convective transport from geothermal borehole heat exchangers embedded in a fluid-saturated porous medium. *Renewable Energy*, 196:328–342, 2022. doi: [10.1016/j.renene.2022.06.089](https://doi.org/10.1016/j.renene.2022.06.089).
- [7] M.A. Sheremet, M.S. Astanina, and I. Pop. MHD natural convection in a square porous cavity filled with a water-based magnetic fluid in the presence of geothermal viscosity. *International Journal of Numerical Methods for Heat & Fluid Flow*, 28(9):2111–2131, 2018. doi: [10.1108/HFF-12-2017-0503](https://doi.org/10.1108/HFF-12-2017-0503).
- [8] I.V. Kapyrin. Assessment of density driven convection effect on the dynamics of contaminant propagation on a deep well radioactive waste injection disposal site. *Journal of Computational and Applied Mathematics*, 392:113425, 2021. doi: [10.1016/j.cam.2021.113425](https://doi.org/10.1016/j.cam.2021.113425).
- [9] F. Agostini, C. Sundberg, and R. Navia. Is biodegradable waste a porous environment? A review. *Waste Management & Research*, 30(10):1001–1015, 2012. doi: [10.1177/0734242X12452444](https://doi.org/10.1177/0734242X12452444).
- [10] Y.W. Tsang and K. Pruess. A study of thermally induced convection near a high-level nuclear waste repository in partially saturated fractured tuff. *Water Resources Research*, 23(10):1958–1966, 1987. doi: [10.1029/WR023i010p01958](https://doi.org/10.1029/WR023i010p01958).
- [11] C. Hu, M. Sun, Z. Xie, L. Yang, Y. Song, D. Tang, and J. Zhao. Numerical simulation on the forced convection heat transfer of porous medium for turbine engine heat exchanger applications. *Applied Thermal Engineering*, 180:115845, 2020. doi: [10.1016/j.applthermaleng.2020.115845](https://doi.org/10.1016/j.applthermaleng.2020.115845).
- [12] V.A. Maiorov, L.L. Vasil'ev, and V.M. Polyayev. Porous heat exchangers—classification, construction, application. *Journal of Engineering Physics*, 47(3):1110–1123, 1984. doi: [10.1007/BF00873730](https://doi.org/10.1007/BF00873730).
- [13] S. Javed, N. Deb, and S. Saha. Natural convection and entropy generation inside a square chamber divided by a corrugated porous partition. *Results in Engineering*, 18:101053, 2023. doi: [10.1016/j.rineng.2023.101053](https://doi.org/10.1016/j.rineng.2023.101053).
- [14] K. Al-Farhany, A. Abdulkadhim, H.K. Hamzah, F.H. Ali, and A. Chamkha. MHD effects on natural convection in a U-shaped enclosure filled with nanofluid-saturated porous media with two baffles. *Progress in Nuclear Energy*, 145:104136, 2022. doi: [10.1016/j.pnucene.2022.104136](https://doi.org/10.1016/j.pnucene.2022.104136).
- [15] N.M. Basher, O.R. Alomar, and I.A. Mohamed. Impact of using single heated obstacle on natural convection inside porous cavity under non-Darcy flow and thermal non-equilibrium model: A comparison between horizontal and vertical heated obstacle arrangements. *International Communications in Heat and Mass Transfer*, 133:105925, 2022. doi: [10.1016/j.icheatmasstransfer.2022.105925](https://doi.org/10.1016/j.icheatmasstransfer.2022.105925).
- [16] A.A. Yousif, O.R. Alomar, and A.T. Hussein. Impact of using triple adiabatic obstacles on natural convection inside porous cavity under non-Darcy flow and local thermal non-equilibrium model. *International Communications in Heat and Mass Transfer*, 130:105760, 2022. doi: [10.1016/j.icheatmasstransfer.2021.105760](https://doi.org/10.1016/j.icheatmasstransfer.2021.105760).
- [17] X. Jiang, M. Hatami, A. Abderrahmane, O. Younis, B.M. Makhdom, and K. Guedri. Mixed convection heat transfer and entropy generation of MHD hybrid nanofluid in a cubic porous cavity with wavy wall and rotating cylinders. *Applied Thermal Engineering*, 226:120302, 2023. doi: [10.1016/j.applthermaleng.2023.120302](https://doi.org/10.1016/j.applthermaleng.2023.120302).

- [18] S.E. Ahmed and Z.A.S. Raizah. Magnetic mixed convection of a Casson hybrid nanofluid due to split lid driven heat generated porous triangular containers with elliptic obstacles. *Journal of Magnetism and Magnetic Materials*, 559:169549, 2022. doi: [10.1016/j.jmmm.2022.169549](https://doi.org/10.1016/j.jmmm.2022.169549).
- [19] Z.A.S. Raizah, A.M. Aly, and S.E. Ahmed. Natural convection flow of a nanofluid-filled V-shaped cavity saturated with a heterogeneous porous medium: Incompressible smoothed particle hydrodynamics analysis. *Ain Shams Engineering Journal*, 12(2):2033–2046, 2021. doi: [10.1016/j.asej.2020.09.026](https://doi.org/10.1016/j.asej.2020.09.026).
- [20] R. Mohebbi, S.A.M. Mehryan, M. Izadi, and O. Mahian. Natural convection of hybrid nanofluids inside a partitioned porous cavity for application in solar power plants. *Journal of Thermal Analysis and Calorimetry*, 137:1719–1733, 2019. doi: [10.1007/s10973-019-08019-9](https://doi.org/10.1007/s10973-019-08019-9).
- [21] J.S. Chordiya and R.V. Sharma. Conjugate natural convection in a fluid-saturated porous enclosure with two solid vertical partitions. *Heat Transfer—Asian Research*, 47(8):1031–1047, 2018. doi: [10.1002/htj.21364](https://doi.org/10.1002/htj.21364).
- [22] A.A. Alnaqi and A.A. Al-Rashed. Heat transfer in a porous cavity divided by a solid wall. *International Journal of Applied Engineering Research*, 13(19):14048–14059, 2018.
- [23] J.S. Chordiya and R.V. Sharma. Numerical study on effect of corrugated diathermal partition on natural convection in a square porous cavity. *Journal of Mechanical Science and Technology*, 33(5):2481–2491, 2019. doi: [10.1007/s12206-019-0445-4](https://doi.org/10.1007/s12206-019-0445-4).
- [24] J.S. Chordiya and R.V. Sharma. Numerical analysis on the effect of wavy partitions on natural convection in porous enclosure. *ASME Journal of Heat Transfer*, 142(9):092601, 2020. doi: [10.1115/1.4047502](https://doi.org/10.1115/1.4047502).
- [25] J.S. Chordiya and R.V. Sharma. Conjugate natural convection in porous medium with a thick square-wave partition. *Journal of Thermal Science and Engineering Applications*, 13(1):011006, 2021. doi: [10.1115/1.4046607](https://doi.org/10.1115/1.4046607).
- [26] J.S. Chordiya and R.V. Sharma. Numerical study on the effects of multiple internal diathermal obstructions on natural convection in a fluid-saturated porous enclosure. *Archive of Mechanical Engineering*, 65(4):553–578, 2018. doi: [10.24425/ame.2018.125442](https://doi.org/10.24425/ame.2018.125442).
- [27] J. Chordiya and R.V. Sharma. Numerical analysis of the longitudinal size of the partition on natural convection heat transfer and fluid flow within a differentially heated porous enclosure. *Heat Transfer*, 52(1):890–910, 2023. doi: [10.1002/htj.22721](https://doi.org/10.1002/htj.22721).
- [28] A. Bejan. On the boundary layer regime in a vertical enclosure filled with a porous medium. *Letters in Heat and Mass Transfer*, 6(2):93–102, 1979. doi: [10.1016/0094-4548\(79\)90001-8](https://doi.org/10.1016/0094-4548(79)90001-8).
- [29] R.J. Gross, M.R. Baer, and C.E. Hickox Jr. The application of flux-corrected transport (FCT) to high Rayleigh number natural convection in a porous medium. In: *International Heat Transfer Conference Digital Library*. Begel House Inc., 1986.
- [30] A.C. Baytas and I. Pop. Free convection in oblique enclosures filled with a porous medium. *International Journal of Heat and Mass Transfer*, 42(6):1047–1057, 1999. doi: [10.1016/S0017-9310\(98\)00208-7](https://doi.org/10.1016/S0017-9310(98)00208-7).
- [31] O.V. Trevisan and A. Bejan. Natural convection with combined heat and mass transfer buoyancy effects in a porous medium. *International Journal of Heat and Mass Transfer*, 28(8):1597–1611, 1985. doi: [10.1016/0017-9310\(85\)90261-3](https://doi.org/10.1016/0017-9310(85)90261-3).